이학석사 학위논문

Cancer theranostic effect of hyaluronic acid-coated graphene oxide targeting oncogenic miR-21

히알루론산이 결합된 그래핀 옥사이드를 이용한 암 유발 유전자 miR-21 표적치료 연구

2015년 6월

서울대학교 융합과학기술대학원

분자의학 및 바이오제약학과

김 한 영

Abstract

Cancer theranostic effect of hyaluronic acid-coated graphene oxide targeting oncogenic miR-21

Han Young Kim

Department of Molecular Medicine and Biopharmaceutical Science

Graduate School of Convergence Science and Technology

Seoul National University

Purpose:

With less availability of antibody-based cancer therapeutic approach, oncogenic nucleic acid-targeting therapy has been spotlighted as new paradigm for cancer therapeutics. However, in vivo delivery issues and uncertainty of therapeutic antisense drug

reaction remain as critical hurdles for successful targeted cancer therapy. Therefore, development of in vivo delivery system and technique to evaluate real antagomir reaction to oncogenic microRNA (miRNA) is necessary to advance the shortcomings of conventional anti-miRNA therapeutics. In this study, we developed in vivo graphene oxide-mediated antagomir delivery nanoplatform to inhibit endogenous miR-21 and monitored the inhibition efficacy of antagomir against miR-21 in cancer-bearing mice.

Method:

Cy3 fluorescent dye-labeled peptide nucleic acid (PNA) containing complementary sequence for microRNA21 (Cy3-PNA21) and scramble sequence (Cy3-PNAscr) were first prepared, and simply mixed with hyaluronic acid-coated graphene oxide (HA-GO) for final formation of HA-GO-PNA21 (HGP21) and HA-GO-PNAscr (HGPscr) complex with quenched fluorescence. For observation of sequence-specific fluorescence recovery, miR-21 mimics and scramble microRNA mimics were each treated to HGP21 and HGPscr. Furthermore, HGP21 and HGPscr were

treated to MDA-MB-231, a malignant human breast cancer cell known as over-expressing hyaluronic acid specific CD44 receptor on its membrane, and also high expression of miR-21. Simultaneously, HGP21 and HGPscr were treated to HeLa cell, a miR-21 low-expressing cell line. Therapeutic effect of HGP21 was evaluated by various experiments including proliferation analysis, migration assay and measurement of apoptotic activity. For in vivo application, MDA-MB-231 tumor xenograft model was established followed by injection of HGP21, HGPscr, and PNA21 (P21) for in vivo miR-21 imaging. Fluorescence image was taken at 1, 3, 6, 24 hr post-injection.

Results:

Fluorescence intensity in Cy3-anti-PNA21 was decreased as HA-GO concentration was increased, showing maximum quenching dose at 0.3 μg. Different dose of miR-21 oligomer treatment gradually recovered the quenched fluorescence signals in HGP21, compared to scramble oligomer treatment or HGPscr with miR-21. When HGP21 was treated into MDA-MB-231 (miR-21 positive) cells, intense cy3 signal was found in the cytoplasmic area, compared to HGPscr-treated group. 2 hr pre-treatment of

free HA to block CD44 resulted in hardly observable Cy3 signal. No fluorescence signal was also observed in HGP21-treated HeLa cells known to show low expression of miR-21. All these in vitro experiments were parallel with flow cytometry results. HGP21-transferred MDA-MB-231 cells revealed therapeutic effect of suppressing cancer proliferation and migration by lowering amount of miR-21. In addition, HGP21 treatment induced high apoptotic activity by recovering PTEN expression. In vivo fluorescence images displayed that intravenously administered HGP21 efficiently targeted the cancer site with intense fluorescence signal in nude mice, compared to HGPscr or PNA21 injected mice. Ex vivo fluorescence image and confocal microscopic data in tumor tissue section supported that HGP21 specifically delivered to tumor and anti-PNA21 was successfully blocked oncogenic miR-21 in vivo.

Conclusions:

In this study, we developed in vivo delivery nanoplatform of anti-miR21 using graphene oxide, and visualized the targeting pattern of therapeutic anti-miR21 to oncogenic miR-21 in vivo. We expect that this system will be readily applicable for in vivo delivery of other

therapeutic anti-microRNAs in wide variety of cancers and could provide promising in vivo nanodevice for antisense oligonucleotide-based cancer theranostics.

Keywords: miR-21, Peptide nucleic acid, Hyaluronic acid, Graphene oxide, Cancer theranostics, Optical imaging, microRNA knockdown

Student Number: 2013-24028

Contents

List of Figures

Introduction

MicroRNAs (miRNAs) are small, non-coding RNAs with 20 to 24 nucleotides which play a key role in gene expression at the post-transcriptional level either by down-regulating their target mRNAs or causing mRNA degradation, and results in regulation of downstream pathway [1-5]. In particular, miR-21 has been recently highlighted from a number of groups, owing to its overexpression in wide variety of cancer types including brain, ovaries, liver, colon and breast. MiR-21 functions as oncogenic miRNA by targeting tumor suppressor gene such as PTEN, BCL-2, and PDCD4. From its role in carcinogenesis, knockdown of miR-21 resulted in inhibition of invasion, proliferation, and migration of breast cancer cells, and also promoted apoptosis in ovarian cancer cells [6, 7].

Weissleder group showed growth inhibition of glioma in vivo by treatment of LNA-antimiR-21 [8]. Furthermore, there are numerous recent reports of miR-21-associated tumorigenesis caused by up-regulation of miR-21, or results related to therapeutic effects by down-regulating miR-21 [9]. Several previous researches showed successful in vivo therapeutics

using anti-miR-21, however, those experiments were performed by a transfection of anti-miR-21 in vitro before an implantation of cancer cells to animal models, showing their limitation considering the real in vivo delivery system. Therefore, the system for delivering anti-miR-21 should be developed. In spite of recent report in delivering anti-miR-21 with nanoparticle, difficulties for enhancing loading capacity of anti-miR-21 and complexity of nanoparticle synthesis still exists. Thus, development of loading high capacity of anti-miR-21 to nanoparticle with simple method is required.

Graphene oxide (GO), an oxidized form of graphene, has two-dimensional sp2 carbon networks which provide a large surface area on both sides of the sheet for the physical adsorption of nucleobases or aromatic compounds. In addition, the electric properties of GO surface allow long-range fluorescence resonance energy transfer (FRET) and can effectively quench the attached fluorescent dye.

Taking these advantages, GO has been widely used as a biosensor for detecting oncogene or protein in cancer cells [10-12], or as theragnostic agent for drug or siRNA delivery in animal tumor models. *Min et al* suggested miRNA detection method via peptide nucleic acid and

nanographene oxide (PANGO) system which provides improved affinity and sensitivity owing to neutral charge of peptide nucleic acid (PNA), compared to negative-charged RNA or DNA causing a repulsion against negative-charged GO [13]. However, the poor stability and aggregation behavior of GO in ionic solution such as PBS or cell medium remained to be challenges for the application as a theranostic agent in vitro and also for in vivo translation. In addition, without any cancer targeting ligand or antibody, GO can be taken up non-specifically by normal cells. For cancer-specific delivery in vivo, we carried out the conjugation of GO with a biopolymer of hyaluronic acid (HA), a CD44 receptor-specific polysaccharide, for stable and target-specific delivery of therapeutic agent [14, 15].

In this study, hyaluronic acid (HA)-graphene oxide (GO) conjugates, with a high loading of dye-labeled peptide nucleic acid (PNA) were developed as a cancer targeted and sequence-based fluorescence switchable nanoplatform for simultaneous detection and inhibition of oncogenic miR-21 (Fig. 1).

Materials and methods

Cell Cultures

MDA-MB-231 cells were cultured in RPMI-1640 (Welgene, Daegu, Korea) containing L-glutamine, supplemented with 10% fetal bovine serum (FBS, Gibco, USA), 100 units/mL penicillin and 100 μg/mL streptomycin at 37 ℃ at 5% CO_2. HeLa cells were maintained in Dulbecco's Modified Eagle's Medium (DMEM) containing 4.5 g/L D-glucose, supplemented with 10% FBS, 1% antibiotics.

MiR-21 detection using HGP complex

HA-GO solution was prepared in test tube as 100 μg/mL, and each fluorescent cy3-PNA probe as 10 μM in distilled water. For validation of complete HGP formation with quenched fluorescence, 40 pmoL of cy3-PNA was mixed with serial concentration of HA-GO solution from 0.1 μg to 0.5 μg. 50 μL of HGP21 and HGPscr complex (PNA: 40 pmoL, HA-GO: 0.3 μg) was mixed with various concentration (5-80 pmoL in 50 μL

distilled water) of either miR-21 or miR-scr. Fluorescence measurement was carried out with fluorometer (Varioskan Flash, Thermo Scientific), with excitation of 550 nm and emission of 570 nm. The fluorescent images of mixtures in 96-well plate were collected using a charge coupled device (CCD) camera of Lumina 2 imaging system (Perkin Elmer, MA, USA). The imaging condition was as follows: exposure time = 2 s, f/stop = 2, and binning = 4. Region-of-interest (ROI)-based measurements of each mixture was calculated with Living Image® software. All mixtures were triplicated.

8 x 10^4 of MDA-MB-231 cells were counted and seeded on 24-well plate. On the next day, HGP21 or HGPscr complex in opti-MEM (HA-GO: 3.75 μg/mL, PNA: 0.5 μM) was treated to the cells. For receptor blocking study, MDA-MB-231 cells were pre-treated with free HA for 1 hr before treatment of HGP complexes. Each HGP complex was treated for 16 hr in serum-free condition and vigorously washed three times with PBS. The cells were fixed with 4% paraformaldehyde and attached to the coverslip using a mounting solution containing 4´,6-diamidino-2-phenylidole. Confocal microscopy images were obtained using LSM 510 (Zeiss, Munich, Germany). Flow cytometric analysis (BD FACS Calibur-2, CA, USA) was performed with cell mixture of each groups. Mixture was analyzed by laser

excitation of 488 nm wavelength, with 530/30 nm emission filters.

qRT-PCR analysis of miR-21

To measure the amount of miR-21 by qRT-PCR, total RNA of MDA-MB-231 cells and HeLa cells were isolated with Trizol reagent (Life Technologies, CA, USA). Initially, miRNA 1st-strand cDNA was synthesized with polyadenylation reaction of total RNA, followed by cDNA synthesis reaction using miRNA 1st-strand cDNA kit (NAME). SYBR green (Takara, Tokyo, Japan)-based quantitive RT-PCR was performed using the 7500 Fast Real-Time PCR System (Applied Biosystems, MA, USA) with prepared cDNA and miR-21 forward primer (TAGCTTATCAGACTGATGTTGA) and universal reverse primer (Agilent Technology, CA, USA).

In vitro antitumor efficacy study of HGP21 complex

Antitumor effect of HGP21 complex was tested with cell viability test, migration assay, and caspase 3/7 activity test. Lipofectamine 2000® was used as positive control for intracellular delivery of PNA21 and PNAscr.

After treatment of HGP21, HGPscr, Lipofectamine-PNA21 (LP21), and Lipofectamine-PNAscr (LPscr), cell proliferation rate of MDA-MB-231 cells was checked using CCK-8 assay kit (Dojindo, Kumamoto, Japan) in every 12 hr until 72 hr post-treatment. For migration assay, MDA-MB-231 cells with more than 90% confluence were scratched with 200 μL pipette tip after 16 hr post-treatment. Cells were scratched and incubated with RPMI-1640 containing 1% FBS for cell starvation and therefore minimizing cell proliferation. Cell image was taken with optical microscopy at 0, 18, 26 hr after starting incubation. To test apoptotic activity of HGP and LP treated MDA-MB-231 cells, caspase 3/7 assay was carried out using capase-Glo® 3/7 assay systems (Promega, USA) at 48 hr post-treatment. Caspase activity was normalized by protein concentration calculated from BCA assay (Thermo Scientific, IL, USA). Absorbance in CCK-8 assay and luminescence in caspase 3/7 assay was both measured with Glomax® multi detection systems (Promega, USA).

Western blot analysis

MDA-MB-231 cells were washed three times with PBS and lysed on the culture dishes using lysis buffer (25mM Tris-HCl, 150mM NaCl, 1% NP-

40, 1% sodium deoxycholate, 0.1% SDS, 1% proteinase inhibitor). Concentration of isolated protein was calculated through BCA method. Total 10 μg of each protein sample was loaded on Nupage® Bis-Tris mini gel (Life Technology, NY, USA) and separated by electrophoresis for 40 minutes with 200 V constant. After electrophoresis, gel was transferred to PVDF membranes for 2 hr, 120 V. Nonspecific binding sites were blocked by incubating with 5% skim milk solution for 2 hr, room temperature. Membranes were then incubated with rabbit mono-clonal PTEN antibody (1:3000) and rabbit ß-actin polyclonal antibody (1:5000), both in 5% BSA solution until next day at 4 ℃. Anti-rabbit secondary antibodies with horseradish peroxidase (1:3000) were treated to the membrane for 2 hr, room temperature. After extensive washing with PBS, protein was visualized by treatment of HRP chemiluminescent substrate (Millipore, MA, USA) and analyzed by FluorChem™ M System (Protein Simple, CA, USA)

Serum stability of HGP complex

Fluorescence intensity of Cy3-PNA and initial HGP complex were used

for measurement of stability in serum. HGP (HA-GO: 0.75 μg) complex was mixed with PBS or human blood serum (1:10 dilution) and incubated in 37 ℃ at 5% CO_2. The mixture of HGP complex added with PBS or serum were measured with fluorometer at 0.5, 1, 2, 5, 30, 60, 180, 360 minutes after addition. Serum stability of each group was calculated by following equation.

$$\left(\frac{\mathrm{RFU}_{\mathrm{Cy3-PNA}} - \mathrm{RFU}_{\mathrm{HGP}}}{\mathrm{RFU}_{\mathrm{Cy3-PNA}} - \mathrm{RFU}_{\mathrm{initial\ HGP}}}\right) \times 100\ (\%)$$

In vivo miR-21 imaging

Five-week-old male Balb/c nude mice, obtained from Orient Bio Inc. (Seongnam, South Korea), were used for in vivo HGP delivery and miR-21 imaging. For establishment of tumor xenograft model, 5 x 10^6 MDA-MB-231 cells were injected subcutaneously. After tumor volume reached 100 mm^3, HGP21 and HGPscr complex dispersed in saline (cy3-PNA: 50 μM, HA-GO: 37.5 μg) were injected intravenously. 50 μM of Cy3-PNA21 without HA-GO was also injected for control. In vivo fluorescence images were collected using Lumina 2 imaging system (Perkin Elmer, MA) at 1, 3, 6, 24 hr of post-injection. After 24 hr, MDA-MB-231 tumors were isolated

and stored in 4 % paraformaldehyde. The imaging condition was as follows: exposure time = 10 s, f/stop = 2, binning = 4, excitation: 570 nm, emission: 620 nm.

Statistical analysis

Results were presented as mean values with standard errors of means (SEM). The Student's *t*-test was conducted to measure P value. The P value which is for less than 0.05 is accepted for statistical significance.

Results

Synthesis of HA-GO

We first prepared GO sheets by using a modified Hummers' method previously reported [17]. Hyaluronic acid was conjugated on GO surface by using ADH as a linker. HA-GO was finally prepared with a final concentration of 0.25 mg/mL in distilled water. We analyzed characteristics of HA-GO compared to GO (Fig. 2). First, HA-GO or GO was dispersed in distilled water, PBS, and cell medium for observation of their stability and solubility. After 1 day, GO showed colloidal aggregation in PBS and cell medium. In contrast, HA-GO showed its stable dispersion in both PBS and cell medium. Next, we examined their morphology and size distribution by AFM microscopy and DLS measurement. GO showed the mean size of 79.5 nm and HA-GO was 120.9 nm in its mean size. The zeta potential value of each nanomaterial was measured about -37.6 mV and -30.5 mV. All these data indicate successful conjugation of HA to GO surface and final synthesis of HA-GO.

Sequence-specific fluorescence recovery of HGP complex

We evaluated the fluorescence quenching ability of prepared HA-GO. We designed Cy3 dye-conjugated PNA21 probe with sequence complementary to miRNA-21 and Cy3-PNAscr as a negative control. The 40 pmol of Cy3-PNA21 was prepared and serial concentration of HA-GO ranging from 0.1 μg to 0.5 μg in 200 μL was simply mixed in room temperature. After 20 minutes, fluorescence of each group was measured with fluorometer, and the result showed complete quenching at 0.3 μg. (Fig. 3A). Cy3-PNA21 was attached on HA-GO surface in 40 pmol : 0.3 μg ratio. We optimized HGP nanocomplex with above ratio, then examined its sequence specific fluorescence recovery. First, HGP21 (Cy3-PNA21 attached in HA-GO) and HGPscr (Cy3-PNAscr in HA-GO) was prepared, then miR-21 or miR-scr was added to each HGP21 and HGPscr nanocomplex. After reaction, high fluorescence recovery of cy3-PNA was shown only in HGP21 mixed with miR-21, which are complementary to each other (Fig. 3B). ROI analysis data also showed 5-6 fold-increase of fluorescence intensity in HGP21 mixed with miR-21, compared to other groups (Fig. 3C).

In vitro detection of miR-21 using HGP complex in breast cancer cells

In order to monitor miR-21 in living cell, MDA-MB-231, miR-21 over-expressing cells were treated with HGP21 and HGPscr (0.5 nM of PNA). Images of the cells showed that the intracellularly delivered HGP induced the increase in fluorescence signal of cy3 dye with different intensity in each group. HGP21-treated cells showed higher fluorescence intensity compared to HGPscr-treated cells, indicating cy3-PNA21 attached on HA-GO surface reacted with endogenous miR-21 and detached from the HA-GO surface, resulted in fluorescence emission (Fig. 4A). In contrast, PNAscr loaded on HA-GO was unable to react with endogenous miR-21 owing to its mismatched sequence. Interestingly, MDA-MB-231 with pre-treatment of free HA for blocking CD44 receptor, did not showed any fluorescence signal in both HGP21 and HGPscr treated cells. This result indicates that blocking CD44 receptor causes decrease of HA-GO internalization to cell cytoplasm, consistent with other reports [18, 19]. Furthermore, miR-21 low expressing HeLa cells treated with either HGP21 or HGPscr induced no changes in fluorescence of the cells (Fig. 4B). The fluorescence intensity of cells treated with either HGP21 or HGPscr was

quantified by flow cytometric analysis, and consistent result with confocal microscopy images was observed (Fig. 4C, 4D).

Therapeutic effect of breast cancer cells by targeting miR-21

As HGP complex showed sequence-specific fluorescence signal in miR-21 over-expressing cell, we speculated that PNA21 from HA-GO has hybridized with endogeneous miR-21 and blocked the downstream in tumorigenesis, and may show the therapeutic effect. During the several experiments for validating therapeutic effects of HGP complex, we used Lipofectamine® as transfection agent for positive control which is typical method for gene delivery.

First, for evaluation of miR-21 inhibition, qRT-PCR was performed from total RNA extracted from MDA-MB-231 cells treated with HGP21, HGPscr, and Lipofectamine-PNA (LP21 and LPscr). As shown in Fig. 5A, HGP21-treated cells showed ~90% decrease of miR-21 compared to HGPscr-treated cells. In addition, capability of HGP21 in miR-21 inhibition showed no difference from LP21. This result indicates that HA-GO mediated PNA delivery shows similar inhibition effect for oncogenic miR-21 knockdown, compared to conventional lipofectamine-based

transfection.

PTEN, a tumor suppressor gene, is one of the target genes of oncogenic miR-21. Reported from previous studies, inhibition of miR-21 via treatment of HGP21 results in induction of PTEN expression. As expected, isolated protein from HGP21-treated MDA-MB-231 cells showed higher PTEN expression compared to HGPscr-treated cells (Fig. 5B). We expected that higher PTEN expression would result in decreased proliferation rate, invasiveness. Therefore, we performed proliferation assay of MDA-MB-231 cells after treatment of HGP and LP. MDA-MB-231 treated with HGP21 showed decreased proliferation rate until 72 hr post-treatment compared to HGPscr-treated cells, as shown in Fig. 5C. Furthermore, invasiveness test was performed with treatment of HGP, and through the cell scratch technique. Cell medium was changed to 1% FBS supplementation to minimize cell proliferation, and Fig. 5D shows decreased invasiveness in HGP21-treated MDA-MB-231 cell at 18 and 26 hr post-treatment. According to reports that knockdown of miR-21 promotes apoptosis, we evaluated apoptotic activity of HGP- and LP-treated MDA-MB-231 by measurement of caspase 3/7 activity. Data was normalized with protein concentration of each group calculated by BCA

assay. Consistent with previous proliferation, migration test, HGP21- and LP21-treated MDA-MB-231 cell showed higher caspase 3/7 activity, indicating induction of apoptosis by HGP21 treatment (Fig .5E).

PET imaging of breast cancer-bearing mouse and fluorescence imaging of its overexpressed endogenous miR-21 by delivery of HGP21

HGP21 complex showed its capability of imaging for oncogenic miR-21 expression, and simultaneous knockdown effect against miR-21. According to previous reports that HA-GO has affinity with MDA-MB-231 cell which is known to over-express CD44 receptor, we speculated that HGP complex would be capable of targeting MDA-MB-231 tumor in vivo, and detect the amount of oncogenic miR-21 after receptor mediated endocytosis. For examination of tumor targeting efficacy and biodistribution of HGP21 complex, we labeled the HGP21 complex with ^{64}Cu radioisotope to follow up via PET imaging system. C-terminal of Cy3-PNA oligonucleotide was modified from carboxyl group to azido group, and ADIBO-PEG-

NOTA for ^{64}Cu chelation was prepared. Click chemistry method was used to conjugate Cy3-PNA and ADIBO-PEG-NOTA. Synthesized ^{64}Cu-PNA21 was simply mixed with HA-GO for complete formation of ^{64}Cu-HGP21, which was intravenously injected to tumor model. In vivo PET images were taken at 1, 6, 24 hr post-injection, and as shown in Fig. 6A, ^{64}Cu-HGP21 and ^{64}Cu-HGPscr both specifically targeted the tumor site in nude mice. While both HGP21 and HGPscr were capable of tumor targeting, we expected that only HGP21 injected mice would show fluorescence signal in tumor because of fluorescence recovery based on perfect sequence-match. As expected, HGP21 injected mice showed significantly higher fluorescence intensity in the tumor site compared to HGPscr-and PNA21-injected mice (Fig. 6B). According to region of interest analysis (Fig. 6C), HGP21-injected mice showed more than 5-fold increase of fluorescence signal in tumor site. After sacrifice, organs from each mice group were isolated and visualized separately in florescence imaging system. Fluorescence intensity of each organ was measured by ROI analysis. Despite the accumulation of HGP complex in lung,

liver and spleen as shown in PET images, ROI analysis showed low fluorescence intensity in highly accumulated organs, however, tumor isolated from HGP21 injected mice showed high fluorescence intensity (Fig. 6D). This indicates that HGP21 and HGPscr complex maintain their quenched fluorescence until reaching the tumor site, and fluorescence recovery occurs after intracellular delivery of HGP21 by receptor-mediated endocytosis, followed by reaction with their complementary sequence, an endogenous miR-21. In support of this, tumor was then paraffin-sectioned in 5 μm thickness for histological analysis. To evaluate Cy3-PNA21 from HGP21 complex was detached from HA-GO and induced fluorescence in tumor tissue, we deparaffinized the tumor section and mounted in cover slide with DAPI. As a result shown in Fig. 6E, tumor tissue of HGP21 injected mice showed significantly higher Cy3 dye fluorescence compared to HGPscr or Cy3-PNA21 injected mice, consistent with in vivo imaging result.

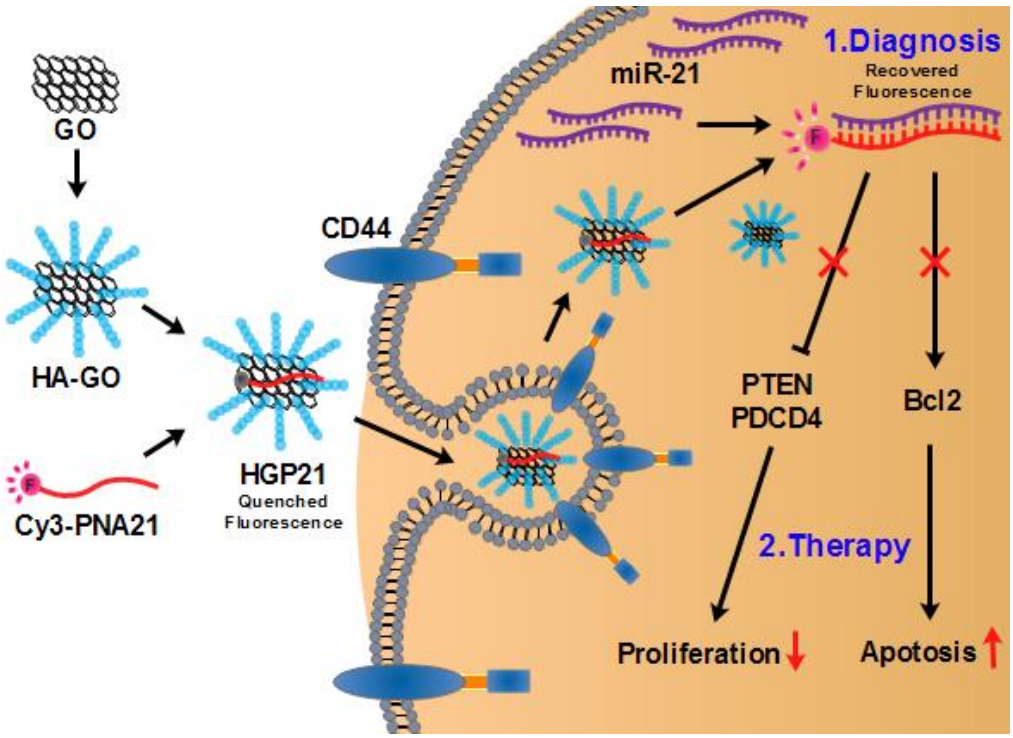

Fig. 1. Schematic illustration of HGP synthesis and its theranostic effect by targeting miR-21.

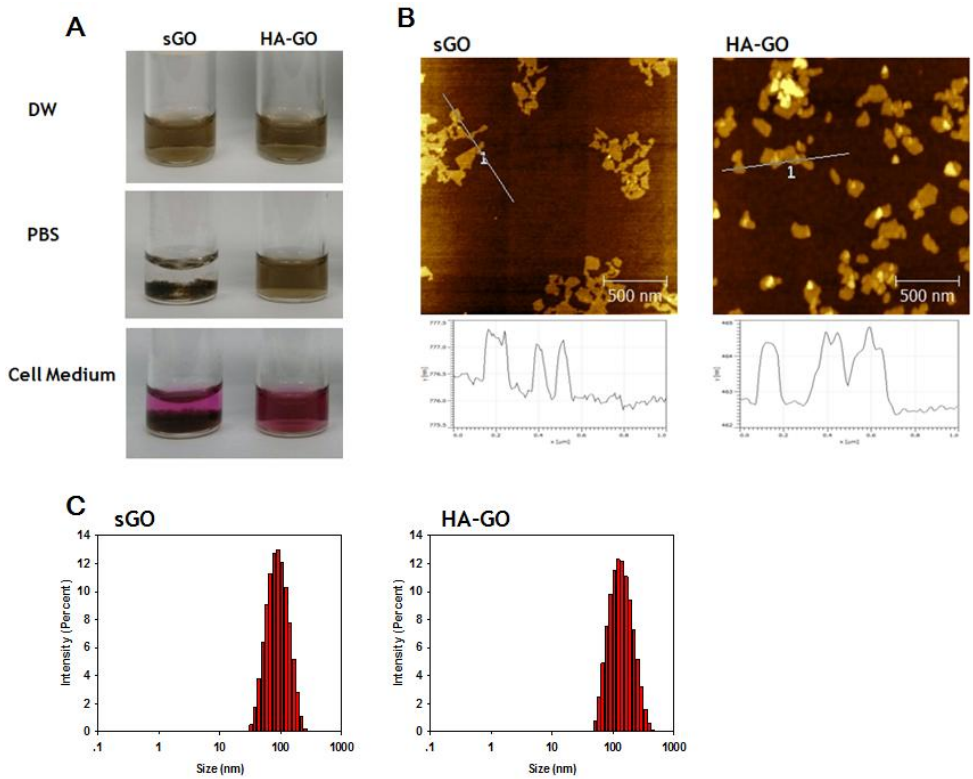

Fig. 2. Characterization of GO and HA-GO in physiological condition. (A) Monodispersity of GO and HA-GO in physiological condition was evaluated by addition of PBS and cell medium. Conjugation of HA on GO surface resulted in improvement of stability in PBS and cell medium. (B) Morphology, lateral size, and height of GO and HA-GO were observed in AFM microscopy. (C) Size distribution of GO and HA-GO was analyzed by DLS measurement.

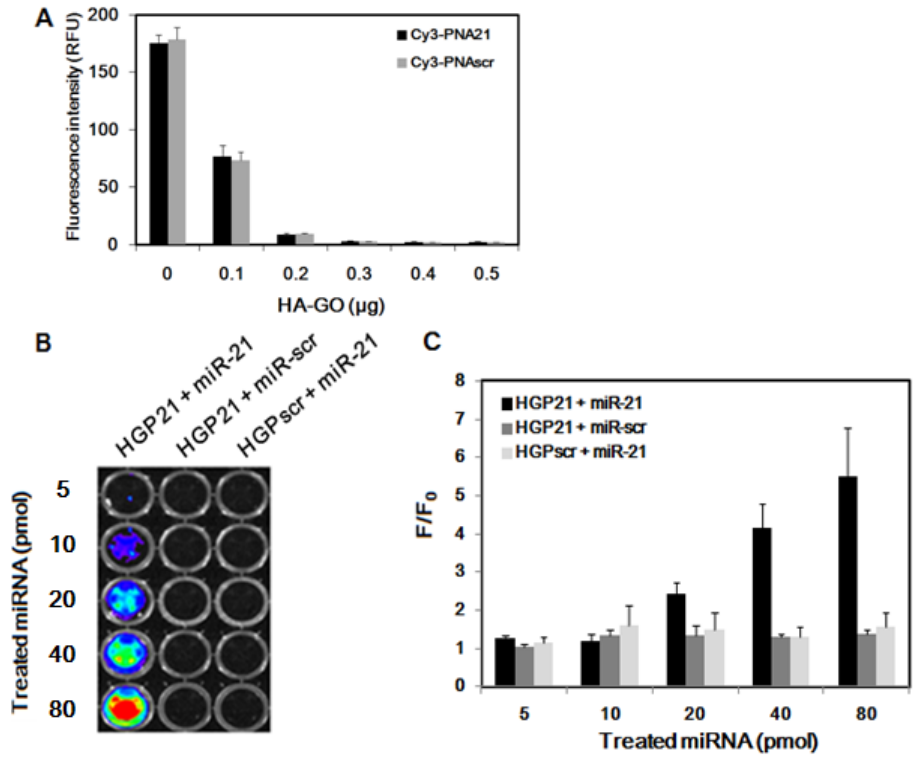

Fig. 3. Sequence-specific detection of miR-21 using HGP21 complex.

(A) Fluorescent signal of Cy3-PNA21 and Cy3-PNAscr (40 pmol) was dose-dependently quenched by addition of HA-GO. As both Cy3-PNA21 and Cy3-PNAscr completely quenched with 0.3 μg HA-GO, HGP complex was synthesized with ratio of 13.3 pmol : 0.1 μg (Cy3-PNA : HA-GO). (B) Fluorescence recovery of HGP21 (PNA 40 pmol, HA-GO 0.3 μg) and HGPscr treated with either miR-21 or miR-scr was observed up to 80 pmol. (C) ROI analysis was represented as F/F_0 (F: Fluorescence intensity after addition of miRNA, F_0: Fluorescence intensity of initial HGP)

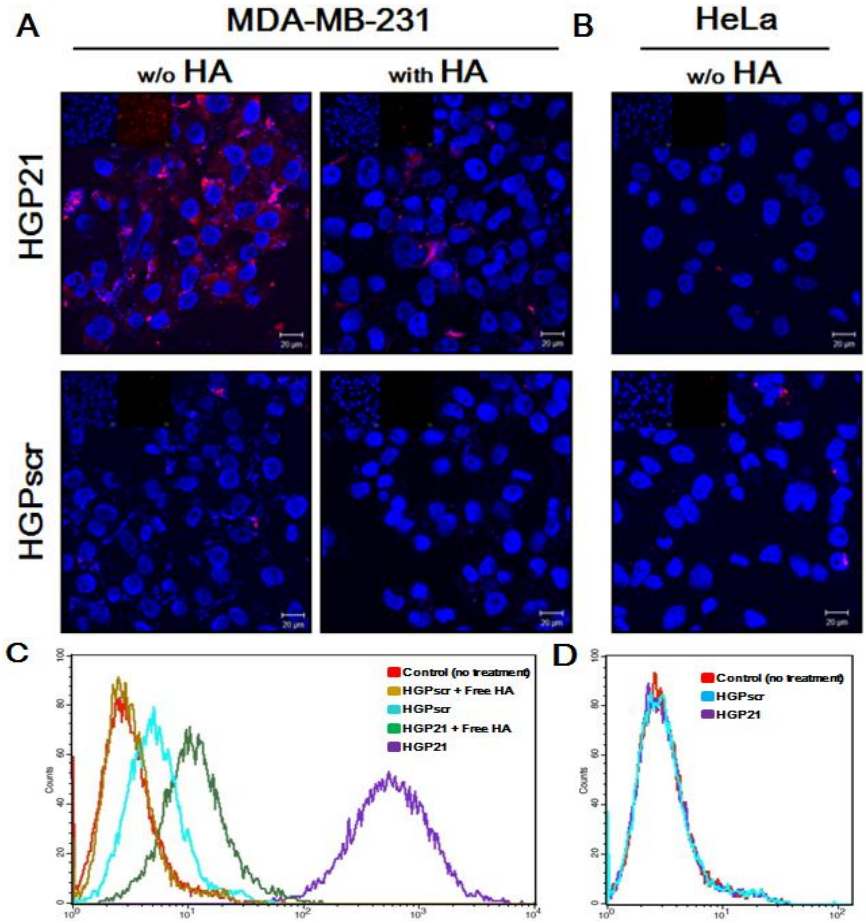

Fig. 4. Fluorescence detection of endogenous miR-21 via treatment of HGP21. (A) MDA-MB-231 cells highly expressing miR-21 were treated with HGP21 or HGPscr (Cy3-PNA 0.5 μM). For blockage of CD44 receptor, free HA (10 mg/mL) was pre-treated for 2 hr. (B) HeLa cells (low expression of miR-21) were treated with HGP21 or HGPscr. (C and D) Flow cytometry analysis was performed for quantitative measurement of fluorescence intensity from (A) and (B)

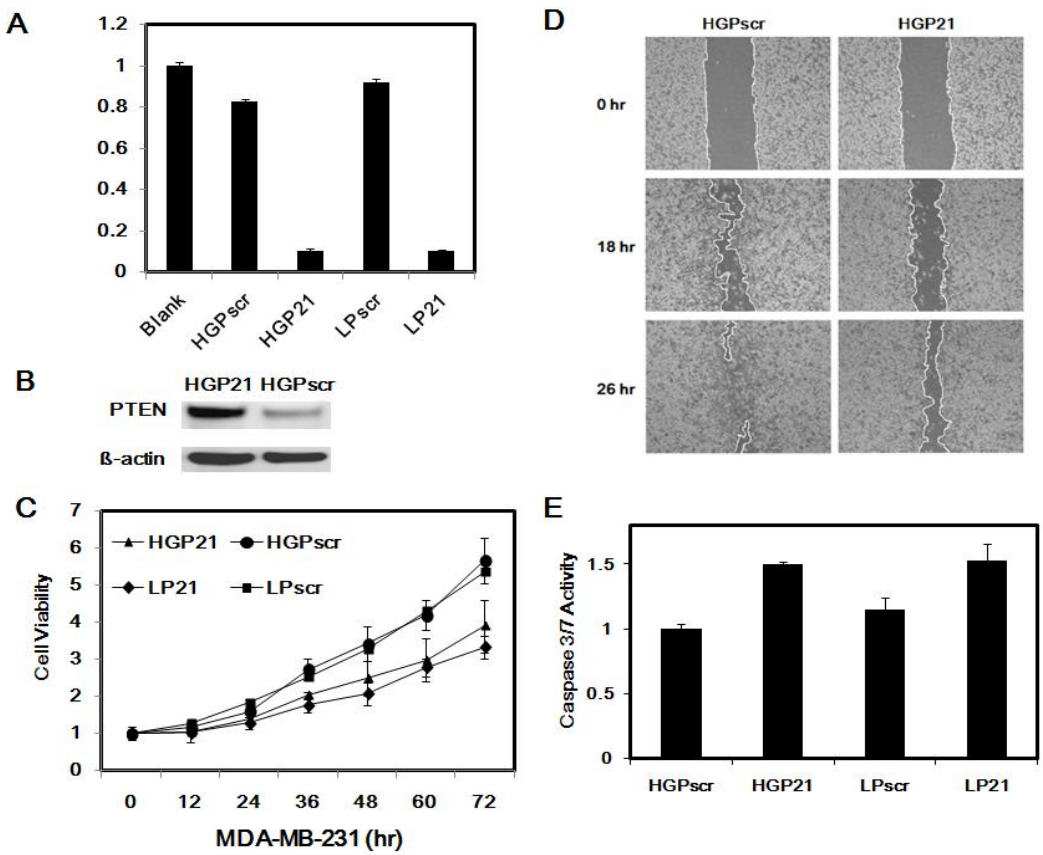

Fig. 5. Evaluation of therapeutic effect of HGP21 to miR-21 over-expressing MDA-MB-231 cell. (A) HGP complex was quantitatively measured with Real-time PCR. Lipofectamine® 2000 was used as positive control for delivery of PNA (LP21 and LPscr). (B) PTEN expression was increased in HPG21-treated MDA-MB231 cancer cells by western blot analysis. (C) Cell proliferation rate in HPG21-treated MDA-MB231 cancer cells was inhibited until 72 hr post-treatment of HGP and LP complex. (D)

Cancer cell invasiveness was observed until 26 hr post-treatment of HGP21 or HGPscr. Cells were scratched with 100 μL pipette tips and medium was changed to 1% FBS supplementation to minimize cell proliferation. MDA-MB231 cells were reduced in their invasiveness in HGP21-treated group. (E) Apoptosis in MDA-MB-231 cells treated with HGP21 complex was induced by examination of caspase 3/7 activity.

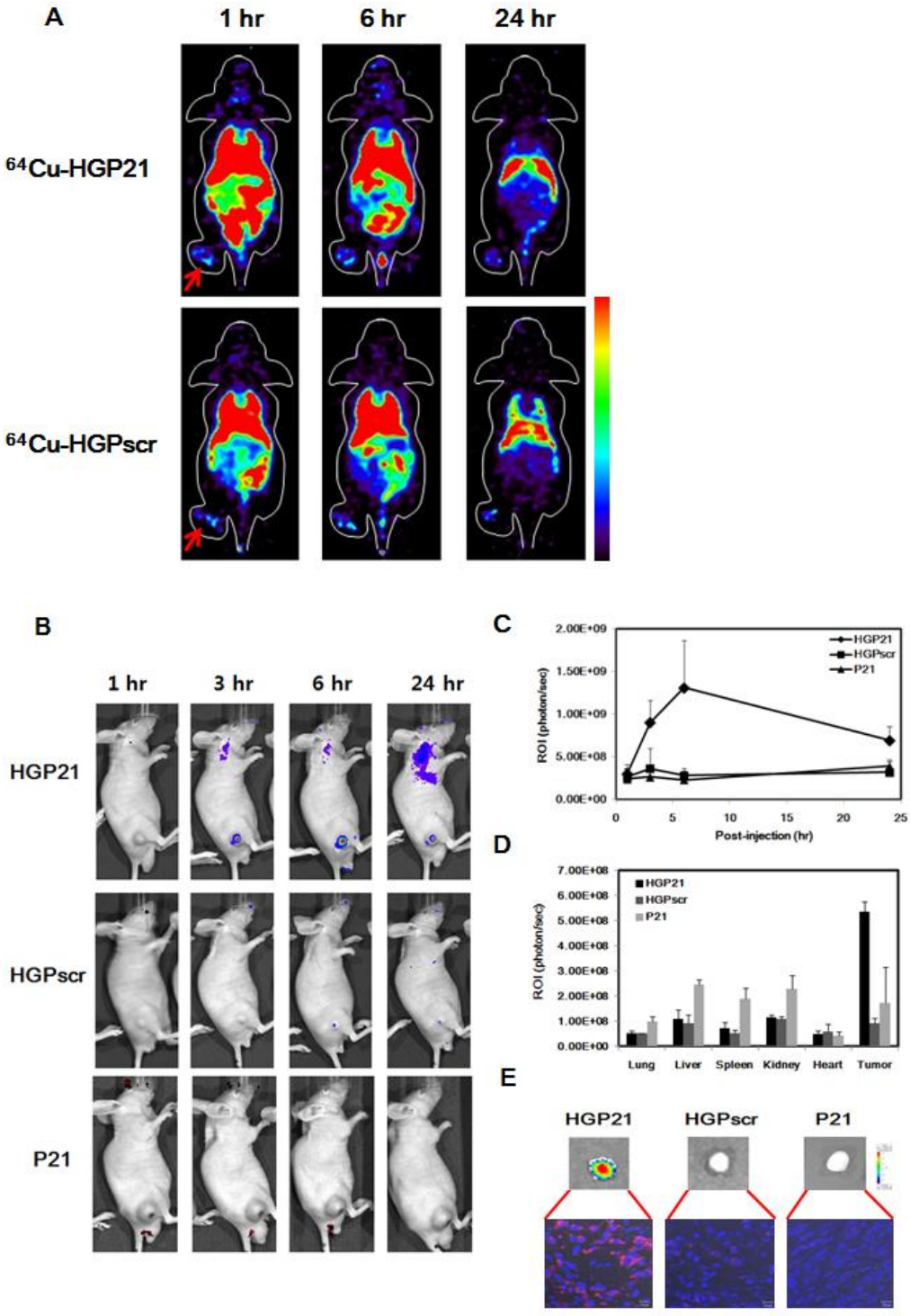
A
1 hr
6 hr
24 hr
64Cu-HGP21
64Cu-HGPscr
B
1 hr
3 hr
6 hr
24 hr
HGP21
HGPscr
P21
C
HGP21
HGPscr
P21
ROI (photon/sec)
Post-injection (hr)
D
HGP21
HGPscr
P21
ROI (photon/sec)
Lung
Liver
Spleen
Kidney
Heart
Tumor
E
HGP21
HGPscr
P21

Fig. 6. In vivo imaging of MDA-MB-231 tumor and its overexpressed miR-21. (A) Serial whole body coronal PET images of MDA-MB-231 tumor-bearing mice were taken at different time points after intravenous injection of ^{64}Cu-HGP21 and ^{64}Cu-HGPscr. The radioactivity of injected ^{64}Cu-HGP21 and ^{64}Cu-HGPscr was detectable in tumor site of nude mouse (B) In vivo fluorescence images in MDA-MB-231 tumor-bearing mouse was taken at 1, 3, 6, 24 hr post-injection of HGP21, HGPscr and P21 (PNA-21 without conjugation of HA-GO was injected as a negative control). (C) Fluorescence intensity of each tumor site was calculated by region of interest analysis. (D) Organs from each group at 24 hour post-injection were isolated, and fluorescence intensity was measured. (E) Ex vivo fluorescence images were taken from isolated MDA-MB-231 tumor and their tissue sections were observed with confocal microscopy (DAPI : nucleus, Red : Cy3-PNA).

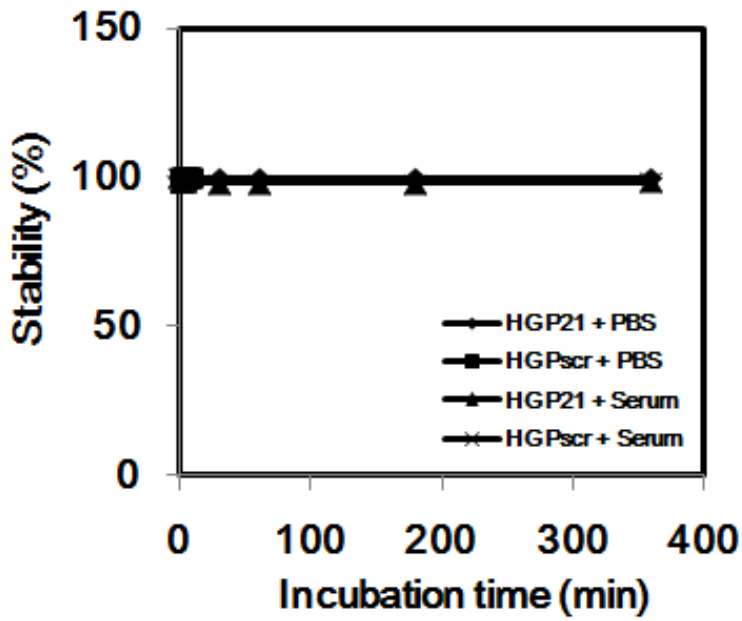

Supplementary Fig. 1. Serum stability test of HPG21 and HPGscr in serum condition up to 6 hr. HGP21 and HGPscr was mixed with syringe-filtered human blood serum and their fluorescence intensities were measured until 6 hr for observation of possible detachment of Cy3-PNA from HA-GO.

Discussion

We demonstrated that fluorescence dye-labeled therapeutic anti-PNA21 can be successfully delivered to the tumor site via loading on HA-GO, and it simultaneously visualized the oncogenic miR-21 expression in cancer xenograft model. Despite several reports showing the capability of GO as a gene or drug delivery cargo, its low monodispersity in physiological conditions such as cell culture medium or blood serum, has remained as a critical issue. Herein, we grafted HA on GO surface to enhance its solubility for avoidance of aggregation in various physiological solutions. Since HA shows strong interaction with CD44, a receptor usually expressed in metastatic breast cancer cell lines, it was also used as a breast cancer targeting moiety.

For conjugation of HA on GO surface, ADH was used as a linker for stable conjugation and for preservation of large area on GO surface. PNA, an oligomer with backbone consisted of continuous peptide bonds, was

reported for its high loading efficiency toward GO surface compared to DNA and RNA which have phosphate-rich backbone. Negative charge from phosphate groups in backbone of DNA and RNA can cause electric repulsion between negatively charged GO surface, and therefore PNA with neutral charge shows higher affinity and enhanced loading efficiency on GO surface with approximately 10-fold increase. PNA binds directly on GO surface via pi-pi interaction between nucleotide base and aromatic ring on GO surface, and therefore the amount of dye-labeled PNA loaded on GO can be maximized when the steric hindrance caused by HA polymer is minimized. We observed no difference of quenching ability between GO and HA-GO, which indicates the conjugation of HA on GO surface did not affect the loading capacity of PNA.

In this study, we observed that HA-GO was capable of receptor-mediated endocytosis in breast cancer cell and intracellularly delivered the anti-miR-21 PNA probe for detection and simultaneous inhibition of oncogenic miR-21, resulting in decreased tumorigenecity. HGP21 with quenched fluorescence entered the cytoplasm of MDA-MB-231 breast cancer cell (miR-21 and CD44 dual positive cell line) by receptor-mediated pathway, and Cy3-PNA21 from the HA-GO surface reacted with the

endogenous miR-21, and this process was highly sequence specific. In support of this, we found no observable fluorescence recovery in HeLa cell, which express 40-fold less miR-21 compared to MDA-MB-231, indicating high sensitivity of HGP21. Since CD44 expression in HeLa cell was comparably equivalent to MDA-MB-231 cell, the higher fluorescence signal showed in MDA-MB-231 cell after HGP21 treatment was due to sequence specificity of PNA21 toward endogenous miR-21 rather than cell internalization efficacy of HA-GO cargo.

As we speculated that the delivered Cy3-PNA21 via HA-GO can act as an antagomir against oncogenic miR-21 and block its downstream pathway, HGP21 treatment resulted in higher PTEN expression and provided cancer therapeutic effect. We observed significant miR-21 knockdown from HGP21 treated MDA-MB-231 cells. Furthermore, HGP21 treated group showed equivalent knockdown effect compared to anti-miR-21 transfected group via Lipofectamine®, a commercial agent which is widely used for effective oligomer transfection. As HGP21 blocked the downstream of oncogenic miR-21, HGP21 treated cells showed suppressed proliferation rate, migration rate, and upregulated cell apoptosis. All this results indicates

that Cy3-PNA21 from HA-GO has successfully detected endogenous miR-21 in quantitative manner, and simultaneously interrupted the carcinogenicity of oncogenic miR-21.

As high solubility and stability is required for in vivo application of synthesized nanomaterials, we examined the conjugation stability of Cy3-PNA probe against HA-GO in serum condition. Consistent with previous studies reported that not only pi-pi interaction, but also hydrogen bonding and van der Waals interaction contribute in strong coupling between oligonucleotide and GO, no observable detachment of cy3-PNA from GO was found until 6 hr after an addition of blood serum. To evaluate the tumor targeting efficacy of HGP complex in tumor xenograft model, we radio-labeled the HGP21 and HGPscr with ^{64}Cu radioisotope and visualized their biodistribution via PET imaging system. C-terminal of PNA oligonucleotide was modified to azido group, and click chemistry method was used for conjugation of ADIBO-PEG-NOTA for chelating ^{64}Cu radioisotope. ^{64}Cu-HGP21 and ^{64}Cu-HGPscr were prepared and intravenously injected into tumor xenograft model. As expected, HGP21 and HGPscr showed similar tumor targeting efficacy, however, only the HGP21-injected mice showed observable fluorescence signal on tumor site,

indicating HGP21 was accumulated in tumor site and recovered its fluorescence in sequence-specific manner, by comparison between HGPscr. Confocal microscopy analysis of isolated tumor tissue showed consistent result that only HGP21-injected mice tumor strongly emitted the Cy3 fluorescence signal. To confirm whether Cy3-PNA21 was stably conjugated to HA-GO in organs except tumor, organs such as lung, liver, spleen, kidney, and heart were isolated and their fluorescence intensities were measured. PET image showed high uptake of HGP21 and HGPscr in liver or spleen compared to tumor site, however, fluorescence intensities in these isolated organs were ignorable. This result can be an evidence of high stability of Cy3-PNA21 against HA-GO in body organs except the MDA-MB-231 tumor which highly expresses miR-21.

In spite of numerous studies for gene delivery using certain type of nanomaterial as a cargo, they typically focused on either detection or inhibition of endogenous genes, and revealed their limitations for further in vivo applications. Here, we showed that dye-labeled PNA probe delivered via HA-GO could not only visualize the endogenous miRNA, but also can inhibit its function and show cancer therapeutic effect. Furthermore, this platform was capable of in vivo multimodal imaging with addition of

simple reaction. We provided the evidence that HGP platform for delivering genes has potential for not only as a new approach of gene delivery system, but also in development of cancer theranostic platform for multimodal imaging and inhibition of overexpressed oncogenes.

References

1. Kosaka *et al*. Circulating MicroRNA in Body Fluid: A New Potential Biomarker for Cancer Diagnosis and Prognosis. Cancer Sci. 2010; 101: 2087–2092.
2. Sun *et al*. MicroRNA: A Master Regulator of Cellular Processes for Bioengineering Systems. Annu. Rev. Biomed. Eng. 2010; 12: 1–27.
3. Erson *et al*. M. MicroRNAs in Development and Disease. Clin. Genet. 2008; 74: 296–306
4. Calin et al. MicroRNA Signatures in Human Cancers. Nat. Rev. Cancer 2006; 6:857–866.
5. He *et al.* Small RNAs with a Big Role in Gene Regulation. Nat. Rev. Genet. 2004; 5: 522–531.
6. Lou *et al*. miR-21 down-regulation promotes apoptosis and inhibits invasion and migration abilities of OVCAR3 cells. Clin Invest Med. 2011;34: E281-E289.
7. Yan *et al*. Knockdown of miR-21 in human breast cancer cell lines inhibits proliferation, in vitro migration and in vivo tumor growth.

Breast Cancer Research. 2011; 13:R2.

8. Cortsten *et al.* MicroRNA-21 Knockdown Disrupts Glioma Growth In vivo and Displays Synergistic Cytotoxicity with Neural Precursor Cell–Delivered S-TRAIL in Human Gliomas. Cancer Res. 2007; 67: 19.
9. Chan *et al.* MicroRNA-21 is an antiapoptotic factor in human glioblastoma cells. Cancer Res. 2005; 65: 6029–33.
10. Wang et al. Aptamer/Graphene Oxide Nanocomplex for *in Situ* Molecular Probing in Living Cells. J. AM. CHEM. SOC. 2010; *132*:9274–9276.
11. Zhang *et al*. Enhanced Chemotherapy Effi cacy by Sequential Delivery of siRNA and Anticancer Drugs Using PEI-Grafted Graphene Oxide. Small. 2011; 7:460–464.
12. Park *et al.* A graphene oxide-based platform for the assay of RNA synthesis by RNA polymerase using a fluorescent peptide nucleic acid probe. Chem. Commun. 2013;49:9203.
13. Ryoo *et al*. Quantitative and Multiplexed MicroRNA Sensing in Living Cells Based on Peptide Nucleic Acid and Nano Graphene Oxide (PANGO). ACS Nano. 2013; 7:5882-5891.

14. Park *et al*. Reducible Hyaluronic Acid−siRNA Conjugate for Target Specific Gene Silencing. Bioconjugate Chem. 2013; 24:1201−1209
15. Li *et al*. Hyaluronic acid-conjugated graphene oxide/photosensitizer nanohybrids for cancer targeted photodynamic therapy. J. Mater. Chem. B, 2013; 1:1678.
16. Wu *et al*. Hyaluronic acid conjugated graphene oxide for targeted drug delivery. Carbon. 2014; 6:379 –389
17. Hummers *et al*. Preparation of Graphitic Oxide. J. Am. Chem. Soc. 1958; 80:1339.
18. Son *et al*. Self-Assembled Polymeric Micelles Based on Hyaluronic Acid-g-Poly(d,l-lactide-co-glycolide) Copolymer for Tumor Targeting. Int. J. Mol. Sci. 2014; 15:16057-16068.
19. Jung *et al*. Nano graphene oxide–hyaluronic acid conjugate for target specific cancer drug delivery. RSC Adv. 2014; 4:14197-14200.